

Color octet potential to three loops

Chihaya Anzai,¹ Mario Prausa,¹ Alexander V. Smirnov,² Vladimir A. Smirnov,³ and Matthias Steinhauser¹

¹*Institut für Theoretische Teilchenphysik, Karlsruhe Institute of Technology (KIT), 76128 Karlsruhe, Germany*

²*Scientific Research Computing Center, Moscow State University, 119992 Moscow, Russia*

³*Nuclear Physics Institute, Moscow State University, 119992 Moscow, Russia*

(Received 6 August 2013; published 27 September 2013)

We consider the interaction between two static sources in the color octet configuration and compute the potential to three loops. Special emphasis is put on the treatment of pinch contributions, and two methods are applied to reduce their evaluation to diagrams without pinches.

DOI: [10.1103/PhysRevD.88.054030](https://doi.org/10.1103/PhysRevD.88.054030)

PACS numbers: 12.38.–t, 12.38.Bx

I. INTRODUCTION

The potential energy between two heavy quarks is a fundamental quantity in physics. In fact, the history of computing loop corrections to the potential of quarks forming a color singlet configuration goes back to the mid 1970s with the idea to describe a bound state of heavy colored objects in analogy to the hydrogen atom [1]. One-loop corrections were computed shortly afterward in Refs. [2,3]. The two-loop corrections were only evaluated toward the end of the 1990s by two groups [4–6], and about five years ago, the three-loop corrections were considered in Refs. [7–9], again in two independent calculations.

In this paper we consider the potential in momentum space, which we define as

$$V^{[c]}(|\vec{q}|) = -4\pi C^{[c]} \frac{\alpha_s(|\vec{q}|)}{\vec{q}^2} \left[1 + \frac{\alpha_s(|\vec{q}|)}{4\pi} a_1^{[c]} + \left(\frac{\alpha_s(|\vec{q}|)}{4\pi} \right)^2 a_2^{[c]} + \left(\frac{\alpha_s(|\vec{q}|)}{4\pi} \right)^3 \times \left(a_3^{[c]} + 8\pi^2 C_A^3 \ln \frac{\mu^2}{\vec{q}^2} \right) + \dots \right], \quad (1)$$

where $C_A = N_c$ and $C_F = (N_c^2 - 1)/(2N_c)$ are the eigenvalues of the quadratic Casimir operators of the adjoint and fundamental representations of the $SU(N_c)$ color gauge group, respectively. The strong coupling α_s is defined in the $\overline{\text{MS}}$ scheme, and for the renormalization scale, we choose $\mu = |\vec{q}|$ in order to suppress the corresponding logarithms. The general results, both in momentum and coordinate space, can be found in Appendix A.

In Eq. (1) we have introduced the superscript $[c]$, which indicates the color state of the quark-antiquark system. In Refs. [4–9] only the singlet configurations ($c = 1$) have been considered, which is phenomenologically most important. However, quarks in the fundamental representation can also combine to a color octet state. At tree level and one-loop order, only the overall color factor changes from $C^{[1]} = C_F$ to $C^{[8]} = C_F - C_A/2$. Starting from two loops [10,11], the coefficients $a_i^{[c]}$ get additional

contributions. In this paper we compute $a_3^{[8]}$ and compare the result to $a_3^{[1]}$ [7–9].

The term proportion to $\ln \mu^2$ in Eq. (1) has its origin in an infrared divergence, which has been subtracted minimally. It appears for the first time at three-loop order [12] and is canceled against the ultraviolet divergence of the ultrasoft contributions, which have been studied in Refs. [13–15]. For the resummation of leading and next-to-leading ultrasoft logarithms, we refer to Refs. [16–18]. As anticipated in Eq. (1), the ultrasoft contribution for the color-singlet and color-octet cases differs only by the overall color factor, which is confirmed by our explicit calculation.

Let us for completeness mention that it is possible to generalize the concept of the heavy-quark potential to generic color sources, which in principle can also be in the adjoint representation of $SU(3)$ as, e.g., the gluino in supersymmetric theories. Various combinations of quark, squark, and gluino bound state systems were considered in Ref. [11], and the corresponding potential has been evaluated up to two loops.

A further generalization of the three-loop corrections to $V^{[1]}$ has been considered in Ref. [19], where it is still assumed that the heavy sources form a color singlet state; however, the colour representation is kept general.

The remainder of the paper is organized as follows. In the next section, we explain in detail how we treat the diagrams involving pinches. Afterward, we present our results in Sec. III and conclude in Sec. IV.

II. CALCULATION

As compared to the singlet case, the calculation of the octet potential is substantially more complicated, which is connected to the occurrence of so-called pinch contributions as shall be discussed in the following. Pinch contributions occur in those cases in which a deformation of the integration contour, needed to circumvent poles in the complex plane of the zero-component of the integration momentum, is not possible.

For illustration let us consider the planar ladder diagram in Fig. 1(a). Since the momentum transfer q between the

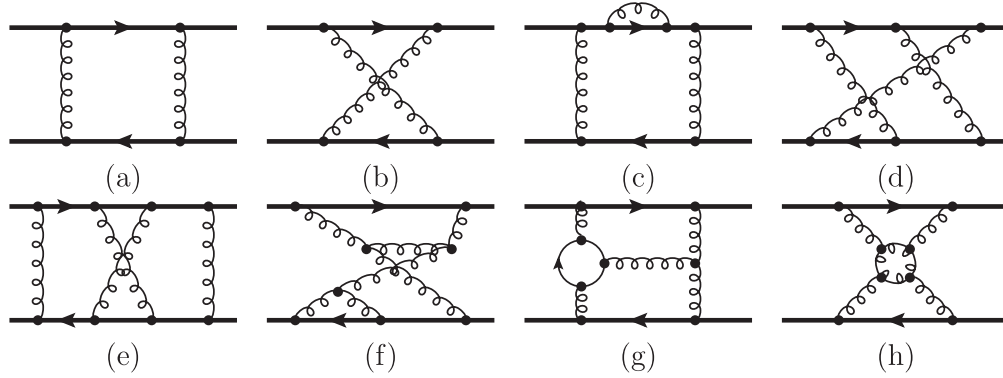


FIG. 1. Feynman diagrams up to three-loop order contributing to $V^{[c]}$. Thick lines represent static quarks, thin solid lines represent massless fermions, and curled lines represent gluons.

heavy quarks is spacelike and the static propagators only contain the energy component of the momentum, we obtain for the loop integral the expression

$$\int d^D k f(k, \vec{q}) \frac{1}{(k_0 + i0)(k_0 - i0)}, \quad (2)$$

where $f(\vec{q})$ collects all prefactors and the contribution from the gluon propagators, and $D = 4 - 2\epsilon$ is the space-time dimension.

There are several possibilities to treat the one-loop diagram in Eq. (2) and obtain a relation to a well-defined integral. For example, it is possible to apply the principle value prescription

$$\frac{1}{(k_0 + i0)(k_0 - i0)} \rightarrow \frac{1}{2} \left[\frac{1}{(k_0 + i\epsilon)^2} + \frac{1}{(k_0 - i\epsilon)^2} \right], \quad (3)$$

which is valid in the soft region for the integration momenta. With the help of Eq. (3), it is possible to treat all contributions involving pinches in one-loop momentum [10,11,20]. The application to diagrams with two or more pinch contributions in one diagram, a situation that appears at two loops and beyond, is not obvious.

Another possibility is based on the fact that in QED with only one (heavy) lepton pair, the potential between the fermion and antifermion is given by the tree-level term (see, e.g., the discussions in Refs. [7,21]), which means that the loop corrections are exactly canceled by the iteration terms of lower-order contributions. The latter arise from the fact that the potential is proportional to the logarithm of the quark-antiquark four-point amplitude which has to be expanded in the coupling constant. Translating this knowledge to QCD means that the sum of all one-loop contributions proportional to C_F^2 has to vanish, which in turn leads to the graphical equation¹

¹We denote the static quarks by horizontal thick lines and the massless modes by thin lines connecting the color sources.

$$\square = \frac{1}{2} (\Gamma)^2 - \text{X}, \quad (4)$$

In this way the planar-ladder contribution can be replaced by the crossed ladder, which is free of pinch contributions. The same method has successfully been applied at two loops [10,11,20] [see Ref. [20] for the two-loop analogue of Eq. (4)].

In the following we provide a general prescription for the treatment of the pinch contributions, which works to all loop orders and for an arbitrary number of involved propagators. We formulate the algorithm in a way that is convenient for our application. Alternative formulations can be found in Refs. [2,21].

It is convenient to formulate the algorithm in coordinate space. Using the Feynman rules from Appendix B, the one-loop ladder diagram in Fig. 1(a) takes the form

$$g_s^4 \int_{-\frac{T}{2}}^{\frac{T}{2}} dw_0 \int_{-\frac{T}{2}}^{\frac{T}{2}} dx_0 \int_{-\frac{T}{2}}^{\frac{T}{2}} dy_0 \int_{-\frac{T}{2}}^{\frac{T}{2}} dz_0 \theta(x_0 - w_0) \theta(z_0 - y_0) \times D_{00}(w_0 - y_0, \vec{r}) D_{00}(x_0 - z_0, \vec{r}), \quad (5)$$

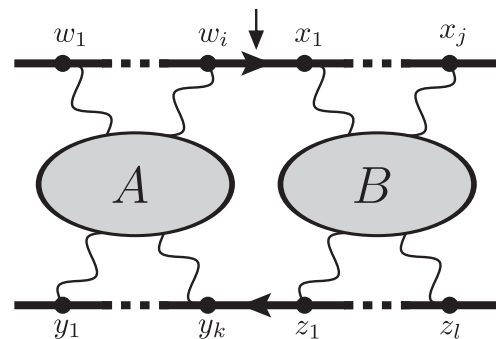


FIG. 2. Generic Feynman diagram involving a pinch contribution. The blobs A and B may contain further pinches, which are treated recursively (see the description of the algorithm). The arrow indicates where the static line is cut at first.

where the color structure has been ignored. In Eq. (5) the integration over the spacial components has been performed, and the θ functions of the vertices have been used to restrict the integration limits of the temporal integrals to $[-T/2, T/2]$. Note that $\theta(x_0 - w_0)$ refers to the upper and $\theta(y_0 - z_0)$ to the lower source line. In analogy one obtains for the generic diagram in Fig. 2 the following combination of θ functions:

$$\theta(w_2^0 - w_1^0) \dots \theta(w_i^0 - w_{i-1}^0) \theta(x_1^0 - w_i^0) \times \theta(x_2^0 - x_1^0) \dots \theta(x_j^0 - x_{j-1}^0). \quad (6)$$

A crucial ingredient to the algorithm described below is the cut of a static propagator. This is equivalent to setting the corresponding propagator to unity; i.e., the associated θ function in Eq. (6) is set to one. Actually, the omission of

$\theta(x_1 - w_i)$ from Eq. (6) (see also Fig. 2) relaxes the original conditions on the zero components

$$w_1^0 < \dots < w_i^0 < x_1^0 < \dots < x_j^0 \quad (7)$$

to

$$w_1^0 < \dots < w_i^0 \wedge x_1^0 < \dots < x_j^0. \quad (8)$$

The latter is satisfied by all Feynman diagrams, which are obtained from the original one by permutations of vertices in the upper source line as long as the order of the vertices involving w 's and x 's is kept. Thus, the result for the cut diagram is obtained by summing all such contributions. Let us illustrate this mechanism by the following three-loop diagram:

$$\overline{\text{XXXX}} = \text{XX} + \text{XX} + \text{XX} + \text{XX} + \text{XX} + \text{XX}. \quad (9)$$

The procedure for cutting an antisource propagator is, of course, in close analogy.

We are now in the position to describe the algorithm, which can be applied to all diagrams involving pinch contributions. The output of the algorithm is equations that relate pinch diagrams to diagrams without pinches. The latter can be computed along the lines of Refs. [7–9]. In all steps QED-like color factors are assumed; the multiplication with the proper color factor happens after applying the obtained relations. In parallel to the description of the algorithm, we illustrate its principle of operation on explicit two- and three-loop examples.

- (1) Consider a diagram with a pinch. In case there is more than one pinch, the following steps have to be applied to each one consecutively. In case more than one source or antisource propagator is involved [see, e.g., Fig. 1(c)], the operations are performed for the most left and most right propagator, and the resulting equations are added.
- (2) Express the pinch diagram by the corresponding diagram with a cut source propagator and the remaining contributions according to Eq. (9).

For our three-loop example, the corresponding equation looks like the following:

$$\text{XXXX} = \overline{\text{XXXX}} - \text{XX} - \text{XX} - \text{XX} - \text{XX} - \text{XX}. \quad (10)$$

- (3) Replace the diagram with a cut source propagator by the diagram in which both the source and antisource propagators are cut and the remaining contributions that are obtained in analogy to step 1. Write the diagram with two cuts as a product of lower-order contributions.

The application of these rules to our example leads to

$$\begin{aligned} \text{XXXX} &= (\overline{\text{XX}})^2 \\ &- \text{XX} - \text{XX} - \text{XX} - \text{XX} - \text{XX} \\ &- \text{XX} - \text{XX} - \text{XX} - \text{XX} - \text{XX}. \end{aligned} \quad (11)$$

- (4) In a next step, the diagrams with a cut in the source propagator have to be treated. This is done by replacing them by the sum of diagrams obtained by considering all allowed permutations of the source vertices.

In our example this leads to

$$\begin{aligned}
 \text{XX} &= (\text{X})^2 \\
 &- 6 \text{X}_1 - 4 \text{X}_2 - 4 \text{X}_3 - 4 \text{X}_4 \\
 &- 4 \text{X}_5 - 2 \text{X}_6 - 2 \text{X}_7 - 2 \text{X}_8 \\
 &- 2 \text{X}_9 - 2 \text{X}_{10} - 2 \text{X}_{11} - \text{X}_{12} .
 \end{aligned} \tag{12}$$

- (5) Solve the resulting equation for the considered pinch diagram.
 In our example the original diagram appears on the right-hand side with a negative sign. This finally leads to

$$\begin{aligned}
 \text{XX} &= \frac{1}{2} (\text{X})^2 \\
 &- 3 \text{X}_1 - 2 \text{X}_2 - 2 \text{X}_3 - 2 \text{X}_4 \\
 &- 2 \text{X}_5 - \text{X}_6 - \text{X}_7 - \text{X}_8 \\
 &- \text{X}_9 - \text{X}_{10} - \text{X}_{11} .
 \end{aligned} \tag{13}$$

Note that all diagrams on the right-hand side of this equation are either products of lower-order contributions or are free of pinches and can thus be computed in the standard way.

- (6) It might be that during the described procedure, scaleless integrals appear that are set to zero within dimensional regularization. This is, in particular, true for nonamputated diagrams.
 (7) It is advantageous to add diagrams with the same color factor before applying the described algorithm since in some cases the pinch diagram appears on the right-hand side and are symmetric to the original one; however, step 2 cannot be performed.

As an example consider the two two-loop diagrams, which can be written as

$$\begin{aligned}
 \text{II} &= \text{I} \cdot \text{X} - 3 \text{X}_1 - 2 \text{X}_2 - 2 \text{X}_3 - \text{X}_4 , \\
 \text{XI} &= \text{I} \cdot \text{X} - 3 \text{X}_1 - 2 \text{X}_2 - 2 \text{X}_3 - \text{II} .
 \end{aligned} \tag{14}$$

In this version the equations cannot be used. However, the sum of the equations leads to

$$\text{II} + \text{XI} = \text{I} \cdot \text{X} - 3 \text{X}_1 - 2 \text{X}_2 - 2 \text{X}_3 . \tag{15}$$

- (8) In case there are still pinch contributions on the right-hand side of the equation, the described procedure is applied iteratively.

Consider, e.g., the two-loop ladder diagram, which, after applying the above steps once, leads to

$$\text{III} = \frac{1}{3} \text{I} \cdot \text{II} - \frac{2}{3} (\text{II} + \text{XI}) - \frac{1}{3} \text{X}_1 - \frac{1}{3} \text{X}_2 . \tag{16}$$

Using Eq. (15) and the one-loop relation (4) results in the equation

$$\text{III} = \frac{1}{6} (\text{I})^3 - \text{I} \cdot \text{X} + 2 \text{X}_1 + \text{X}_2 + \text{X}_3 . \tag{17}$$

It is straightforward to implement the described algorithm in a computer program. We have verified that we reproduce the two-loop results in the literature [10,11,20]. Furthermore, we have verified the exponentiation of the singlet potential up to three loops, and we have checked

that all iteration terms predicted from lower-order contributions are reproduced.

Sample Feynman diagrams contributing to $V^{[8]}$ up to three loops are shown in Fig. 1. We generate the amplitudes with the help of QGRAF [22] and process the output further

using Q2E and EXP [23,24] in order to arrive at FORM-readable results. At that point projectors are applied, traces are taken, and the scalar products in the numerator are decomposed in terms of denominator factors. The resulting scalar expressions are mapped to the integral families defined in Refs. [25–28].

The algorithm used for the treatment of the pinch contributions described above is applied to the output file of QGRAF. While adding the results of all diagrams the obtained relations are applied, and thus the sum is expressed in terms of well-defined integrals.

The computation of the integrals proceeds along the lines of Refs. [7–9]. In particular we use FIRE [29,30] to reduce the integrals to a minimal set, the so-called master integrals. Actually, only of the order of one hundred integrals remains to be reduced after using the tables generated for the computation of the three-loop singlet contribution. They are quite simple and require only a few days of CPU time.

We managed to express the final result for $a_3^{[8]}$ in terms of the same 41 master integrals as $a_3^{[1]}$. Thus, our final result only contains three coefficients (of the ϵ expansion), which are not yet known analytically. Details on the computation of the master integrals can be found in Refs. [26–28,31]. For most of the integrals, even explicit results are provided. For example, the 14 master integrals containing a massless one-loop subdiagram can be found in Ref. [28], and 16 integrals among the most complicated ones are provided in Ref. [27].

We have performed a second calculation of $a_3^{[8]}$, which is described in the following. The calculation of the loop integrals is based on Refs. [9,19], and for the treatment of the pinch contributions, we follow Refs. [32,33]. The basic idea outlined in these references is that the color factor of the diagrams without pinch is changed in such a way that the pinch contribution is taken into account. At the same time, the pinch diagrams are set to zero.

To reach this goal, we define for a color diagram x ,

$$E(x) := C(x) - \sum_{d \in \text{Dec}'(x)} T^{-n(d)} E(d), \quad (18)$$

which corresponds to Eq. (4) of Ref. [32]. In this equation $\text{Dec}'(x)$ represents the set of nontrivial decompositions of x , and $n(d)$ is the number of webs² in d . T equals N_c for the singlet case and $N_c C_F$ for the octet case.

Each Feynman diagram F can be expressed in terms of a product of the color factor $C(F)$ and the momentum space integral $I(F)$. If the color factor $C(F)$ of each diagram is replaced by the new color factor $E(F)$ calculated with the help of Eq. (18), all contributions from iterations will be eliminated. Moreover, $E(F)$ is zero for all pinch diagrams, and hence their evaluation is not needed anymore.

Let us for illustration consider the contribution from the one-loop planar and crossed ladder diagrams of Figs. 1(a) and 1(b). For the octet potential, we can write

$$\delta V_{\text{ladder}}^{[8],(1)} = I \left(\text{Diagram 1(a)} \right) \times \frac{1}{N_c C_F} \left(\text{Diagram 1(a)} \right) + I \left(\text{Diagram 1(b)} \right) \times \frac{1}{N_c C_F} \left(\text{Diagram 1(b)} \right), \quad (19)$$

where the color factors $C(F)$ are presented in graphical form after the factor $1/(N_c C_F)$. If one now replaced $C(F)$ by $E(F)$ and used Eq. (18), one obtains

$$\begin{aligned} V_{\text{ladder}}^{[8],(1)}|_{C \rightarrow E} &= I \left(\text{Diagram 1(a)} \right) \times \frac{1}{N_c C_F} \left[\left(\text{Diagram 1(a)} \right) - \frac{1}{N_c C_F} \left(\text{Diagram 1(a)} \right)^2 \right] \\ &\quad + I \left(\text{Diagram 1(b)} \right) \times \frac{1}{N_c C_F} \left[\left(\text{Diagram 1(b)} \right) - \frac{1}{N_c C_F} \left(\text{Diagram 1(a)} \right)^2 \right] \\ &= I \left(\text{Diagram 1(a)} \right) \times 0 + I \left(\text{Diagram 1(b)} \right) \times \frac{1}{N_c C_F} \left[\left(\text{Diagram 1(b)} \right) - \left(\text{Diagram 1(a)} \right) \right], \end{aligned}$$

which is equivalent to the relation (4) obtained with the method described above.

We want to remark that $V^{[8]}$ is gauge independent since this is the case for the ultrasoft contribution, which has to be added to arrive at a physical result. For this reason we

decided to use Feynman gauge for the practical calculations, and thus we refrain from using a general QCD gauge parameter. In the results that we present below, both methods described in this section lead to the same final expressions, which is a strong check for their correctness.

III. RESULTS FOR $V^{[8]}$

In this section we present results for the coefficients $a_i^{[c]}$ in Eq. (1) for $SU(N_c)$ with a generic number of colors, N_c .

²A web is a set of gluons that cannot be partitioned without cutting at least one of its lines, and a decomposition d of a set of gluon lines is a classification of the lines into webs such that each line is precisely in one web [32]. See Ref. [32] for examples.

Let us for convenience repeat the one- and two-loop results, which read (the octet results were obtained in Refs. [10,11])

$$\begin{aligned}
a_1^{[1]} &= \frac{31}{9} C_A - \frac{20}{9} T_F n_l, \\
a_2^{[1]} &= \left(\frac{4343}{162} + 4\pi^2 - \frac{\pi^4}{4} + \frac{22}{3} \zeta(3) \right) C_A^2 \\
&\quad - \left(\frac{1798}{81} + \frac{56}{3} \zeta(3) \right) C_A T_F n_l \\
&\quad - \left(\frac{55}{3} - 16\zeta(3) \right) C_F T_F n_l + \left(\frac{20}{9} \right)^2 T_F^2 n_l^2, \\
a_1^{[8]} &= a_1^{[1]}, \quad a_2^{[8]} = a_2^{[1]} + N_c^2 \pi^2 (\pi^2 - 12). \quad (20)
\end{aligned}$$

It is remarkable that the difference between the singlet and octet contribution at two loops involves only π^2 and π^4 terms.

At three-loop order, it is convenient to decompose the coefficient in the form

$$a_3^{[c]} = a_3^{[c,(3)]} n_l^3 + a_3^{[c,(2)]} n_l^2 + a_3^{[c,(1)]} n_l + a_3^{[c,(0)]}, \quad (21)$$

where n_l is the number of light quarks. For the first two coefficients, we have

$$\begin{aligned}
a_3^{[1,(3)]} &= -\left(\frac{20}{9} \right)^3 T_F^3, \\
a_3^{[1,(2)]} &= \left(\frac{12541}{243} + \frac{368\zeta(3)}{3} + \frac{64\pi^4}{135} \right) C_A T_F^2 \\
&\quad + \left(\frac{14002}{81} - \frac{416\zeta(3)}{3} \right) C_F T_F^2, \\
a_3^{[8,(3)]} &= a_3^{[1,(3)]}, \quad a_3^{[8,(2)]} = a_3^{[1,(2)]}. \quad (22)
\end{aligned}$$

For the coefficients $a_3^{[c,(1)]}$ and $a_3^{[c,(0)]}$, we expect a similar feature as in the two-loop result of Eq. (20), and thus we write

$$\begin{aligned}
a_3^{[1,(1)]} &= -709.717 C_A^2 T_F + \left(-\frac{71281}{162} + 264\zeta(3) + 80\zeta(5) \right) \\
&\quad \times C_A C_F T_F + \left(\frac{286}{9} + \frac{296\zeta(3)}{3} - 160\zeta(5) \right) C_F^2 T_F \\
&\quad - 56.83(1) \frac{d_F^{abcd} d_A^{abcd}}{N_A} \\
&= -367.319 N_c^2 + 17.3611(7) - 12.597(2) \frac{1}{N_c^2}, \\
a_3^{[8,(1)]} &= a_3^{[1,(1)]} + \delta a_3^{[8,(1)]}, \\
a_3^{[1,(0)]} &= 502.24(1) C_A^3 - 136.39(12) \frac{d_F^{abcd} d_A^{abcd}}{N_A} \\
&= -17.049(7) N_c + 499.396 N_c^3, \\
a_3^{[8,(0)]} &= a_3^{[1,(0)]} + \delta a_3^{[8,(0)]}, \quad (23)
\end{aligned}$$

with

$$\begin{aligned}
\delta a_3^{[8,(1)]} &= 6.836(1) + 40.125 N_c^2, \\
\delta a_3^{[8,(0)]} &= -97.579(16) N_c^3. \quad (24)
\end{aligned}$$

By comparing Eq. (24) with the results in Eq. (23) expressed in terms of N_c , one observes that the coefficients of n_l/N_c^2 and N_c are identical for the singlet and octet cases, and differences only occur in $n_l N_c^2$, the N_c -independent n_l term, and the N_c^3 contribution. In this context it is interesting to present the complete result for $a_3^{[8,(1)]}$, which reads

$$\begin{aligned}
a_3^{[8,(1)]} &= -327.193 N_c^2 + \frac{66133}{648} - \frac{112\pi^2}{9} - \frac{272\zeta(3)}{3} \\
&\quad + \frac{8\pi^4}{3} - \frac{32\pi^2\zeta(3)}{3} + 20\zeta(5) - 12.597(2) \frac{1}{N_c^2}. \quad (25)
\end{aligned}$$

In contrast to the singlet case in Eq. (23), it is possible to obtain an analytic result for the N_c -independent part.

Unfortunately, the quantities $\delta a_3^{[8,(0)]}$ and $\delta a_3^{[8,(1)]}$ are only available numerically. Thus, it is not immediately possible to check the analytic structure of the difference between the singlet and octet coefficient. Nevertheless, it is possible to show that it contains a factor π^2 , a feature that is also observed at two-loop order [10,11] and for $\mathcal{N} = 4$ supersymmetric Yang–Mills theories [20]. The proof of this claim is based on the observation that the master integrals that are present in the expressions for $\delta a_3^{[8,(1)]}$ and $\delta a_3^{[8,(0)]}$ are of the form

$$I = \iiint \frac{d^D k}{(4\pi)^D} \frac{d^D p}{(4\pi)^D} \frac{d^D l}{(4\pi)^D} \frac{1}{k_0 + i0} \frac{1}{p_0 + i0} f(k, p, l, q), \quad (26)$$

where q is the external momentum. The integrand has the special property that one can find variable transformations of k , p , and l , which leave the form invariant except for the static propagators in front of $f(k, p, l, q)$. In fact, one can show that the following relations hold:

$$\begin{aligned}
I &= \iiint \frac{d^D k}{(4\pi)^D} \frac{d^D p}{(4\pi)^D} \frac{d^D l}{(4\pi)^D} \frac{1}{-k_0 + i0} \frac{1}{p_0 + i0} f(k, p, l, q) \\
&= \iiint \frac{d^D k}{(4\pi)^D} \frac{d^D p}{(4\pi)^D} \frac{d^D l}{(4\pi)^D} \frac{1}{k_0 + i0} \frac{1}{-p_0 + i0} f(k, p, l, q) \\
&= \iiint \frac{d^D k}{(4\pi)^D} \frac{d^D p}{(4\pi)^D} \frac{d^D l}{(4\pi)^D} \frac{1}{-k_0 + i0} \frac{1}{-p_0 + i0} f(k, p, l, q). \quad (27)
\end{aligned}$$

Adding the four representations of I leads to

$$\begin{aligned}
I &= \frac{1}{4} \iiint \frac{d^D k}{(4\pi)^D} \frac{d^D p}{(4\pi)^D} \frac{d^D l}{(4\pi)^D} \left(\frac{1}{k_0 + i0} + \frac{1}{-k_0 + i0} \right) \\
&\quad \times \left(\frac{1}{p_0 + i0} + \frac{1}{-p_0 + i0} \right) f(k, p, l, q). \quad (28)
\end{aligned}$$

TABLE I. Numerical values for the coefficients of $[\alpha_s(\mu = |\vec{q}|)/\pi]^i$ ($i = 1, 2, 3$) of the singlet and octet potential.

n_l	$a_1^{[c]}/4$			$a_2^{[c]}/4^2$		$a_3^{[c]}/4^3$			
	3	4	5	3	4	5	3	4	5
Singlet	1.750	1.472	1.194	16.80	13.19	9.740	81.25	49.39	22.83
Octet	1.750	1.472	1.194	4.973	1.366	-2.087	57.33	31.22	10.41

The expressions in the round brackets can be identified with $(-2\pi i)\delta(k_0)$ and $(-2\pi i)\delta(p_0)$, respectively, which immediately leads to an overall factor π^2 .

In Table I we present numerical results for the coefficients of $(\alpha_s/\pi)^i$ ($i = 1, 2, 3$), both for the singlet and the octet potentials for which, for the number of light quarks, n_l , we choose the values 3, 4, and 5, which correspond to the charm, bottom, and top quark cases, and for the renormalization scale, $\mu = |\vec{q}|$. At two-loop order, one observes a compensation of the relatively large two-loop singlet contribution by the additional term present in the octet case. This term is n_l -independent, which even leads to negative values for $a_2^{[8]}$ for $n_l = 5$. Also at three loops, the additional term is negative for all considered values of n_l and leads to a significant reduction, for $n_l = 5$ by more than a factor 2.

IV. CONCLUSIONS

In this paper we have computed the potential between two heavy quarks in a color-octet configuration to three-loop order. The computation of the underlying integrals profits from the calculation of the singlet potential performed in Refs. [7–9]. However, in contrast to the singlet case, the octet potential receives contributions from diagrams with pinches, which significantly complicates the calculation. We discussed two algorithms that are used to obtain the pinch contributions by reducing the calculation to integrals without pinches.

Our final result is presented in Eqs. (22)–(25). One observes quite some similarity to the singlet result. Actually, expressing the coefficients $a_3^{[1]}$ and $a_3^{[8]}$ in terms of N_c , we observe that two out of five coefficients are identical.

As a physical application of the octet potential, one can think of top quarks produced at hadron colliders in a color-octet state. For the description of the threshold effects, the octet potential serves as a crucial ingredient (see, e.g., Refs. [34,35]). Note, however, that the precision of the current calculations does not yet require three-loop corrections to the potential. In a further possible application, one could use $V^{[8]}$ in order to compare with lattice simulations of the potential (see, e.g., Ref. [36]).

ACKNOWLEDGMENTS

We would like to thank Alexander Penin for carefully reading the manuscript and for useful comments. This

work was supported by DFG through Grant No. SFB/TR 9. The work of A. S. and V. S. was partly supported by the Russian Foundation for Basic Research through Grant No. 11-02-01196.

APPENDIX A: $V^{[c]}$ IN COORDINATE AND MOMENTUM SPACE FOR GENERAL RENORMALIZATION SCALE μ

In coordinate space Eq. (1) generalized to arbitrary values of the renormalization scale reads

$$\begin{aligned} \tilde{V}^{[c]} = & -\frac{C^{[c]}\alpha_s(\mu)}{r} \left[1 + \frac{\alpha_s(\mu)}{4\pi} \tilde{c}_1^{[c]}(\mu r) \right. \\ & + \left(\frac{\alpha_s(\mu)}{4\pi} \right)^2 \tilde{c}_2^{[c]}(\mu r) + \left(\frac{\alpha_s(\mu)}{4\pi} \right)^3 \left(\tilde{c}_3^{[c]}(\mu r) \right. \\ & \left. \left. + \frac{64\pi^2}{3} N_c^3 \ln(\mu r) \right) + \dots \right], \end{aligned} \quad (\text{A1})$$

where

$$\begin{aligned} \tilde{c}_1^{[c]}(\mu r) &= \tilde{a}_1^{[c]} + 8\beta_0 \ln(\mu r e^\gamma), \\ \tilde{c}_2^{[c]}(\mu r) &= \tilde{a}_2^{[c]} + 64\beta_0^2 \left[\ln^2(\mu r e^\gamma) + \frac{\pi^2}{12} \right] \\ &\quad + (32\beta_1 + 16\beta_0 \tilde{a}_1^{[c]}) \ln(\mu r e^\gamma), \\ \tilde{c}_3^{[c]}(\mu r) &= \tilde{a}_3^{[c]} + 512\beta_0^3 \left[\ln^3(\mu r e^\gamma) + \frac{\pi^2}{4} \ln(\mu r e^\gamma) + 2\zeta(3) \right] \\ &\quad + (640\beta_0\beta_1 + 192\beta_0^2 \tilde{a}_1^{[c]}) \left[\ln^2(\mu r e^\gamma) + \frac{\pi^2}{12} \right] \\ &\quad + (128\beta_2 + 64\beta_1 \tilde{a}_1^{[c]} + 24\beta_0 \tilde{a}_2^{[c]}) \ln(\mu r e^\gamma), \end{aligned}$$

and

$$\tilde{a}_1^{[c]} = a_1^{[c]}, \quad \tilde{a}_2^{[c]} = a_2^{[c]}, \quad \tilde{a}_3^{[c]} = a_3^{[c]} + \frac{64\pi^2}{3} N_c^3 \gamma.$$

The corresponding relation in momentum space reads

$$\begin{aligned} V^{[c]} = & -\frac{4\pi C^{[c]}\alpha_s(\mu)}{\vec{q}^2} \left[1 + \frac{\alpha_s(\mu)}{4\pi} c_1^{[c]}(\mu^2/\vec{q}^2) \right. \\ & + \left(\frac{\alpha_s(\mu)}{4\pi} \right)^2 c_2^{[c]}(\mu^2/\vec{q}^2) + \left(\frac{\alpha_s(\mu)}{4\pi} \right)^3 \left(c_3^{[c]}(\mu^2/\vec{q}^2) \right. \\ & \left. \left. + 8\pi^2 N_c^3 \ln \frac{\mu^2}{\vec{q}^2} \right) + \dots \right], \end{aligned}$$

where

$$c_1^{[c]}(\mu^2/\vec{q}^2) = a_1^{[c]} + 4\beta_0 \ln\left(\frac{\mu^2}{\vec{q}^2}\right),$$

$$c_2^{[c]}(\mu^2/\vec{q}^2) = a_2^{[c]} + 16\beta_0^2 \ln^2\left(\frac{\mu^2}{\vec{q}^2}\right) + (16\beta_1 + 8\beta_0 a_1^{[c]}) \ln\left(\frac{\mu^2}{\vec{q}^2}\right),$$

$$c_3^{[c]}(\mu^2/\vec{q}^2) = a_3^{[c]} + 64\beta_0^3 \ln^3\left(\frac{\mu^2}{\vec{q}^2}\right) + (160\beta_0\beta_1 + 48\beta_0^2 a_1^{[c]}) \ln^2\left(\frac{\mu^2}{\vec{q}^2}\right) + (64\beta_2 + 32\beta_1 a_1^{[c]} + 12\beta_0 a_2^{[c]}) \ln\left(\frac{\mu^2}{\vec{q}^2}\right),$$

and




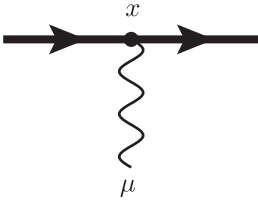
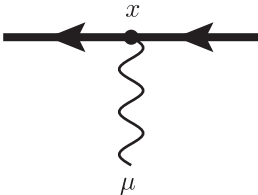
$$\beta_0 = \frac{1}{4} \left[\frac{11}{3} C_A - \frac{4}{3} T_F n_l \right],$$

$$\beta_1 = \frac{1}{16} \left[\frac{34}{3} C_A^2 - 4 C_F T_F n_l - \frac{20}{3} C_A T_F n_l \right],$$

$$\beta_2 = \frac{1}{64} \left[\frac{2857}{54} C_A^3 - \frac{1415}{27} C_A^2 T_F n_l - \frac{205}{9} C_A C_F T_F n_l \right].$$

APPENDIX B: COORDINATE-SPACE FEYNMAN RULES

In coordinate space the QED Feynman rules for a static lepton interacting with a photon read

	$\theta(y_0 - x_0)$	source propagator
	$\theta(y_0 - x_0)$	antsource propagator
	$\frac{g_{\mu\nu}}{4\pi^2(y-x)^2}$	photon propagator
	$-i g_s g^{\mu 0} \delta(\vec{x} - \vec{r}/2) \theta\left(\frac{T^2}{4} - x_0^2\right)$	source vertex
	$i g_s g^{\mu 0} \delta(\vec{x} + \vec{r}/2) \theta\left(\frac{T^2}{4} - x_0^2\right)$	antsource vertex

The relation between the g_s and α_s is given by $\alpha_s = g_s^2/(4\pi)$.

-
- | | |
|---|--|
| [1] T. Appelquist and H.D. Politzer, <i>Phys. Rev. Lett.</i> 34 , 43 (1975). | [9] C. Anzai, Y. Kiyo, and Y. Sumino, <i>Phys. Rev. Lett.</i> 104 , 122003 (2010). |
| [2] W. Fischler, <i>Nucl. Phys.</i> B129 , 157 (1977). | [10] B. A. Kniehl, A. A. Penin, Y. Schroder, V. A. Smirnov, and M. Steinhauser, <i>Phys. Lett. B</i> 607 , 96 (2005). |
| [3] A. Billoire, <i>Phys. Lett.</i> 92B , 343 (1980). | [11] T. Collet and M. Steinhauser, <i>Phys. Lett. B</i> 704 , 163 (2011). |
| [4] M. Peter, <i>Phys. Rev. Lett.</i> 78 , 602 (1997). | [12] T. Appelquist, M. Dine, and I. J. Muzinich, <i>Phys. Rev. D</i> 17 , 2074 (1978). |
| [5] M. Peter, <i>Nucl. Phys.</i> B501 , 471 (1997). | [13] N. Brambilla, A. Pineda, J. Soto, and A. Vairo, <i>Phys. Rev. D</i> 60 , 091502(R) (1999). |
| [6] Y. Schroder, <i>Phys. Lett. B</i> 447 , 321 (1999). | [14] B. A. Kniehl and A. A. Penin, <i>Nucl. Phys.</i> B563 , 200 (1999). |
| [7] A. V. Smirnov, V. A. Smirnov, and M. Steinhauser, <i>Phys. Lett. B</i> 668 , 293 (2008). | |
| [8] A. V. Smirnov, V. A. Smirnov, and M. Steinhauser, <i>Phys. Rev. Lett.</i> 104 , 112002 (2010). | |

- [15] B.A. Kniehl, A.A. Penin, V.A. Smirnov, and M. Steinhauser, *Nucl. Phys.* **B635**, 357 (2002).
- [16] A. Pineda and J. Soto, *Phys. Lett. B* **495**, 323 (2000).
- [17] N. Brambilla, A. Vairo, X. Garcia, I. Tormo, and J. Soto, *Phys. Rev. D* **80**, 034016 (2009).
- [18] A. Pineda and M. Stahlhofen, *Phys. Rev. D* **84**, 034016 (2011).
- [19] C. Anzai, Y. Kiyo, and Y. Sumino, *Nucl. Phys.* **B838**, 28 (2010).
- [20] M. Prausa and M. Steinhauser, *Phys. Rev. D* **88**, 025029 (2013).
- [21] Y. Schroder, Ph.D. thesis, University of Hamburg, 1999.
- [22] P. Nogueira, *J. Comput. Phys.* **105**, 279 (1993).
- [23] R. Harlander, T. Seidensticker, and M. Steinhauser, *Phys. Lett. B* **426**, 125 (1998).
- [24] T. Seidensticker, [arXiv:hep-ph/9905298](https://arxiv.org/abs/hep-ph/9905298).
- [25] A. V. Smirnov, V. A. Smirnov, and M. Steinhauser, Proc. Sci., RADCOR2007 (2007) 024.
- [26] A. V. Smirnov, V. A. Smirnov, and M. Steinhauser, *Nucl. Phys. B, Proc. Suppl.* **183**, 308 (2008).
- [27] A. V. Smirnov, V. A. Smirnov, and M. Steinhauser, Proc. Sci., RADCOR2009 (2010) 075.
- [28] A. V. Smirnov, V. A. Smirnov, and M. Steinhauser, *Nucl. Phys. B, Proc. Suppl.* **205–206**, 320 (2010).
- [29] A. V. Smirnov, *J. High Energy Phys.* **10** (2008) 107.
- [30] A. V. Smirnov and V. A. Smirnov, [arXiv:1302.5885](https://arxiv.org/abs/1302.5885).
- [31] C. Anzai and Y. Sumino, *J. Math. Phys. (N.Y.)* **54**, 033514 (2013).
- [32] J. G. M. Gatheral, *Phys. Lett.* **133B**, 90 (1983).
- [33] J. Frenkel and J. C. Taylor, *Nucl. Phys.* **B246**, 231 (1984).
- [34] K. Hagiwara, Y. Sumino, and H. Yokoya, *Phys. Lett. B* **666**, 71 (2008).
- [35] Y. Kiyo, J. H. Kühn, S. Moch, M. Steinhauser, and P. Uwer, *Eur. Phys. J. C* **60**, 375 (2009).
- [36] G. S. Bali and A. Pineda, *Phys. Rev. D* **69**, 094001 (2004).